MOLECULAR AND CELLULAR BIOLOGY, June 2008, p. 3672–3685 Vol. 28, No. 11
0270-7306/08/$08.00+0 doi:10.1128/MCB.00510-07

In Vivo Study of the Nucleosome Assembly Functions of ASF1 Histone Chaperones in Human Cells[▽]†

Angélique Galvani,‡§ Régis Courbeyrette,§ Morgane Agez, Françoise Ochsenbein, Carl Mann,* and Jean-Yves Thuret*

CEA, iBiTec-S, Gif-sur-Yvette F-91191, France

Received 23 March 2007/Returned for modification 24 May 2007/Accepted 20 March 2008

Histone chaperones have been implicated in nucleosome assembly and disassembly as well as histone modification. ASF1 is a highly conserved histone H3/H4 chaperone that synergizes in vitro with two other histone chaperones, chromatin assembly factor 1 (CAF-1) and histone repression A factor (HIRA), in DNA synthesis-coupled and DNA synthesis-independent nucleosome assembly. Here, we identify mutants of histones H3.1 and H3.3 that are unable to interact with human ASF1A and ASF1B isoforms but that are still competent to bind CAF-1 and HIRA, respectively. We show that these mutant histones are inefficiently deposited into chromatin in vivo. Furthermore, we found that both ASF1A and ASF1B participate in the DNA synthesis-independent deposition of H3.3 in HeLa cells, thus highlighting an unexpected role for ASF1B in this pathway. This pathway does not require interaction of ASF1 with HIRA. We provide the first direct determination that ASF1A and ASF1B play a role in the efficiency of nucleosome assembly in vivo in human cells.

The nucleosome, the basic unit of chromatin, consists of DNA wrapped around an octamer composed of two histones each of the H3, H4, H2A, and H2B families. In this study, we were interested in factors that assemble H3-type histones into chromatin in human cells in vivo. Nucleosome assembly starts with the deposition of histones H3 and H4 on DNA, followed by the loading of histones H2A and H2B (7, 58). The strong electrostatic interactions between DNA and histones preclude the efficient spontaneous assembly of nucleosomes at physiological ionic strength in concentrated solutions (24). During the last 25 years, numerous protein chaperones capable of interacting with histones and facilitating their deposition onto DNA in vitro have been identified (for examples, see references 9, 20, 34, and 52). In vivo, some of these chaperones may have specialized functions in histone folding, storage, delivery to the nucleus, or modification (27) without participating in nucleosome deposition per se. The precise in vivo function and specificity of most histone chaperones thus remain to be determined.

Nucleosome assembly and disassembly occur during DNA replication, repair, transcription, and other events that necessitate access to DNA. In mammals, the major isoforms of the histone H3 family are H3.1, H3.2, and H3.3 (16). H3.1 and H3.2 are expressed and massively incorporated into chromatin during DNA replication in proliferating cells. H3.3 is expressed in all cell cycle phases in proliferating cells, but it is also expressed in quiescent cells (59, 60). Its posttranslational modifications correspond to active gene loci (6, 29), and Ahmad and Henikoff have demonstrated that H3.3, but not H3.1, is deposited in a transcription-dependent manner in *Drosophila melanogaster* cells (3). Moreover, distinct chaperone complexes copurified with H3.3 or H3.1 histones: in vitro, the complexes containing H3.1 are solely competent for DNA synthesis-coupled (SC) assembly, and the complexes containing H3.3 are solely competent for DNA synthesis-independent (SI) assembly (54). The chaperone complexes isolated with H3.1 include the evolutionarily conserved chromatin assembly factor 1 (CAF-1) (54). CAF-1 consists of three subunits (p150, p60, and p48 in human cells) (21, 57) and had previously been isolated as a chaperone for the assembly of newly synthesized H3 and H4 on replicating DNA (52). Through interaction with proliferating cell nuclear antigen (PCNA), CAF-1 localizes to replication foci in S-phase cells (23, 49) and at sites of damaged DNA in UV-treated cells (12). CAF-1 also promotes H3.1 deposition on UV-damaged DNA in vitro (11, 54) and in vivo (42). CAF-1 is essential for viability in early mouse embryos and in murine embryonic stem cells (18). CAF-1 is also essential in humans, as depletion of p60CAF-1 triggers apoptosis in proliferating, but not quiescent, cells (35). Interestingly, in vitro assays showed that extracts from cells depleted of p150CAF-1 or p60CAF-1 are defective in the assembly of nucleosomes on a replicating template (17, 35). Moreover, CAF-1 is directly linked to S-phase progression, as depletion of p150CAF-1 by RNA interference triggers an accumulation of cells in early and mid-S phase (17). CAF-1 is thus a major player in chromatin assembly dependent on DNA synthesis.

SI nucleosome assembly of H3.3 has been characterized during transcription in *Drosophila* cells in vivo, but the histone chaperones involved in this deposition were not identified (3). Chaperone complexes isolated with H3.3 from HeLa cells include the evolutionarily conserved histone repression A factor (HIRA) (54). HIRA is a 110-kDa protein distantly related to p60CAF-1. HIRA belongs to the family of Hir (histone repres-

* Corresponding author. Mailing address: CEA, SBIGeM-Bât. 142, 91191 Gif-sur-Yvette Cedex, France. Phone for Jean-Yves Thuret: 33 1 69 08 64 25. Fax: 33 1 69 08 80 46. E-mail: jean-yves.thuret@cea.fr. Phone for Carl Mann: 33 1 69 08 92 94. Fax: 33 1 69 08 80 46. E-mail: carl.mann@cea.fr.

† Supplemental material for this article may be found at http://mcb.asm.org/.

‡ Present address: INSERM and Université Denis Diderot-Paris7, UMR S 741, Paris F-75005, France.

§ These two authors contributed equally to this work.

▽ Published ahead of print on 31 March 2008.

sion) factors implicated in the coupling of histone synthesis and DNA replication. Indeed, overexpression of HIRA in human cells inhibited histone expression and led to an S-phase arrest (39). Importantly, HIRA is an essential gene for development, as $HIRA^{-/-}$ mice die in utero by day 11 (46). HIRA also promotes the formation of senescence-associated heterochromatic foci (SAHF) in primary human cells (61) and replication-independent assembly of H3.3 to replace protamines by histones throughout the paternal genome of the one-cell embryo (26).

Histone H3.1 and H3.3 complexes purified from HeLa cells contain the human ASF1 (hASF1) proteins (ASF1A and ASF1B) (54). ASF1A and ASF1B belong to the ASF1 family of histone H3/H4 chaperones conserved from yeast to humans. Its founding member was first isolated in *Saccharomyces cerevisiae* as a gene whose overexpression or deletion disrupts silenced chromatin (anti-silencing function 1 [25, 51]). *Drosophila melanogaster* ASF1 was subsequently isolated as a factor that assembles chromatin onto newly replicated DNA in vitro in synergy with CAF-1 (56). *D. melanogaster* ASF1 also colocalizes with active replication forks in *Drosophila* tissue culture cells (48), and in human cells, ASF1A/B is bound through H3/H4 histones to the putative replicative minichromosome maintenance (MCM) helicase complex in chromatin (14). In vertebrate and *Drosophila* cells, depletion of ASF1 leads to an accumulation of cells in S phase (14, 15, 47, 48). In human cells, this inhibition of S-phase progression has been attributed at least in part to a defect in progression of the MCM helicase in the absence of ASF1A/B (14).

ASF1A and ASF1B are 84% identical in their first 156 amino acids but highly divergent in their C termini. In SC assembly, ASF1A and ASF1B appear to have common functions. Indeed, both proteins are present in the complexes copurified with H3.1 that have in vitro SC assembly activity (54). In contrast, ASF1A and ASF1B may function differently in SI assembly, although both proteins copurify with H3.3. Indeed, ASF1A is dramatically enriched in the complexes containing HIRA that are active for SI assembly in vitro (54). Moreover, ASF1A, but not ASF1B, interacts and synergizes with HIRA in vivo for the formation of SAHF (61). Additionally, quiescent human cells contain ASF1A but no detectable ASF1B (43). Recently, Tang et al. studied the ASF1A-HIRA interaction (55). They defined the B domain of HIRA that contains 37 evolutionarily conserved residues that are necessary and sufficient for interaction with the core domain of ASF1A. Interestingly, ASF1A residues involved in binding to the B domain are strictly conserved in ASF1B. Consequently, both ASF1A and ASF1B are able to interact with the B domain. Tang et al. showed that the preferential interaction of HIRA with ASF1A depends on both the N-terminal 30 residues and the C-terminal 50 residues of hASF1 as well as uncharacterized regions of HIRA outside the B domain.

During replicative stress, the amount of newly synthesized histone H3 interacting with hASF1 increases (15). Groth et al. (15) proposed that hASF1 functions as a histone buffer that donates H3/H4 histones to CAF-1 and HIRA, which would be more directly involved in depositing them onto DNA in SC and SI nucleosome assembly pathways, respectively. Indeed, in *Xenopus* egg extracts that contain an abundance of stored histones, ASF1 is dispensable for direct de novo histone deposition in either pathway (45).

In this work, we analyzed the functions of hASF1 in SC and SI assembly of newly synthesized histones H3.1 and H3.3 in live HeLa cells.

MATERIALS AND METHODS

Constructs. Open reading frames (ORFs) of human H3.1 and H3.3 were inserted in pEGFP-N1 (Clontech) or pEGFP-N1 where enhanced green fluorescent protein (EGFP) had been replaced with Flag, Venus, or enhanced cyan fluorescent protein (residues 1 to 172 [CN] or 155 to 238 [CC]). The linker between H3 and the fluorescent protein (FP) was as described previously (22). ASF1A's ORF was inserted in pEGFP-N1 where EGFP was replaced with CN, CC, or mCherry. ASF1A's ORF was rendered insensitive to small interfering RNA (siRNA) A-I by introducing the Ala67 GCA→GCT, Gly68 GGA→GGT, Arg69 AGG→CGA, His70 CAT→CAC, Phe72 TTT→TTC, and Val73 GTA→GTC silent mutations. Mutants were obtained by PCR-mediated mutagenesis (Roche's Expand High Fidelity). All constructs were sequenced.

Cell culture, transfections, and siRNA. HeLa cells were grown in Dulbecco modified Eagle medium (4.5 g of glucose/liter) with 10% fetal bovine serum (Gibco). For synchronization, cells were blocked in mitosis with nocodazole (10 ng/ml, 5 to 6 h). Mitotic cells were harvested by mechanical shake-off and then transfected. For S-phase synchronization, thymidine was added 5 h later (400 μg/ml). The cells were incubated for 13 more hours and then released in S phase by washing the cells with warm medium. siRNAs were designed and synthesized by Invitrogen (Stealth siRNA), and used at final concentrations of 20 nM or 50 nM (Asf1B-II). The sequences of the siRNAs are as follows: ASF1A-I, CCGC AGGAAGGCAUAUGUUUGUAUU; ASF1A-II, GGCAAAGGUUCAGGU GAACAAUGUA; ASF1B-I, CAGCAGGGAGACACAUGUUUGUCUU; and ASF1B-II, CGACCUGGAGUGGAAGAUCAUUUAU. All transfections were done with Lipofectamine 2000 (Invitrogen).

Immunoprecipitations, SDS-PAGE, and Western blotting. HeLa cells (~10e7) were harvested 24 h after transfection, washed in PB buffer (100 mM potassium acetate, 30 mM KCl, 10 mM Na_2HPO_4, 1 mM $MgCl_2$, pH 7.4) and lysed on ice in 1 ml of PB buffer containing 0.2% Triton X-100, 200 mM NaCl, and protease inhibitor (Complete; Roche). The lysate was centrifuged for 1 h at 20,000 × *g*. Anti-GFP microbeads (60 μl; Miltenyi Biotec) were added to the supernatant for 30 min at 4°C. The suspension was loaded on magnetic columns, which were then extensively washed with lysis buffer. The microbeads were harvested, sodium dodecyl sulfate-polyacrylamide gel electrophoresis (SDS-PAGE) 5× loading buffer was added, and the samples were incubated at 95°C for 5 min. After SDS-PAGE, proteins were transferred to nitrocellulose membranes (Schleicher & Schuell) and detected with anti-GFP (Ab290; Abcam), anti-p60CAF-1 (NB500-212A1; Novus Biologicals), anti-hASF1, anti-H3 (Ab1791; Abcam), anti-glyceraldehyde-3-phosphate dehydrogenase (Ab9485; Abcam), or anti-HIRA antibody and horseradish peroxidase-linked secondary antibodies.

Fixed and live cell microscopy. For fixed cell microscopy, cells were grown on three-well glass slides (Cel-line). All incubations were carried out at room temperature. The cells were washed with phosphate-buffered saline (PBS) and fixed in PBS containing 2% formaldehyde. The cells were washed with PBS, incubated in PBS containing 0.2% Triton X-100, and washed (W buffer [PBS containing 0.05% Triton X-100 and 0.1% Tween 20]). The cells were then incubated in filtered PBS containing 0.1% Tween 20 and 5% bovine serum albumin (Sigma) and then incubated with rabbit anti-GFP (Ab290; Abcam), mouse anti-Flag (M2; Sigma), or mouse anti-p150CAF-1 (NB500-207A1; Novus Biologicals) antibodies, washed (buffer W), and finally incubated with Alexa Fluor 488- or Alexa Fluor 594-conjugated secondary antibodies (Molecular Probes). For dual anti-GFP/antibromodeoxyuridine (anti-BrdU) immunolabeling, the cells were first treated with anti-GFP antibodies and anti-rabbit secondary antibodies, then postfixed in PBS containing 2% formaldehyde, and treated with anti-BrdU (clone BU1/75; Harlan Sera Lab) antibodies after 10 min of DNA denaturation in 4 N HCl. The slides were mounted in Prolong Gold (Invitrogen). Image acquisition was done on a Zeiss LSM510 Meta confocal microscope (Plan-Apochromat 63× 1.4-numerical-aperture [NA1.4] objective). For Fig. 2B and C and 3B and C, a representative plane was selected and imaged. For Fig. 2A and 3A, images were taken along the *z* axis for both anti-GFP and anti-p150CAF-1 probes, and a representative plane was selected. For the profile plots, intensity values were determined with ImageJ (http://rsb.info.nih.gov/ij/) and expressed as a percentage of the mean fluorescence value along the line. Colocalization was assessed in at least 500 nuclei from five different experiments; cells where clearly defined foci were unambiguously visible, even on a diffuse background, were

classified as "cells with H3.1-FP foci." Images of mitotic cells stained with anti-GFP were taken along the *z* axis. The whole stack was projected on one plane using ImageJ and the "standard deviation" *z*-projection method.

Bimolecular fluorescence complementation (BiFC) images were acquired with a Leica DMIRE2 (Roper Instrument 1300Y/HS camera, HCX PL APO 63×/NA1.32 objective). At least 85 nuclei were analyzed in two different experiments. For Fig. 2A, the minimum and maximum gray values displayed were set identically for all images. For Fig. 6C, untreated or siRNA-depleted cells were synchronized with a nocodazole block as shown in Fig. 6A, and BrdU (20 μM) was added immediately after shake-off. The cells were fixed in PBS containing 2% formaldehyde and treated with anti-BrdU antibodies 9, 11, and 13 h after shake-off.

Fluorescence recovery after photobleaching (FRAP) experiments were done on cells in culture conditions (plated on Bioptechs ΔT open glass dishes after shake-off of nocodazole-treated cells; incubated in CO_2-independent medium [Gibco] and kept at 37°C with a Bioptechs ΔTC3 Bioptechs controller; evaporation of the medium was prevented by a layer of mineral oil [Sigma]). Photobleaching and image acquisition were carried out on a Zeiss LSM510 Meta confocal microscope with a Plan Neofluar 100× NA1.3 oil immersion objective. The pinhole aperture was set at the maximum value. EGFP was bleached with 100% intensity of lines of 477 nm and 488 nm, and Venus was bleached with lines of 488 nm and 514 nm of a 40-mW laser (argon) set at 85% output power. For each experiment, 200 images were acquired in 88 s. Images were 256 by 200 pixels, 12 bits, acquired in 192 ms, separated by 250 ms. Fifty images were acquired before photobleaching. A 40- by 10-pixels rectangular area was photobleached during 116 ms. Acquisition of the next image started 2 ms later. For all frames, the mean intensity in a background region over time [$I_{bkg}(t)$], the mean intensity in the photobleached area over time [$I_{FRAP}(t)$], and the mean intensity for the whole nucleus over time [$I_{tot}(t)$] were determined. We carried out double normalization (41), which corrects for prebleach intensity, background noise, and photobleaching as follows: $I(t) = [I_{tot}(\text{pre}) - I_{bkg}(t)]/[I_{tot}(t) - I_{bkg}(t)][(I_{FRAP}(t) - I_{bkg}(t)]/[I_{FRAP}(\text{pre}) - I_{bkg}(t)]$, where $I_{tot}(\text{pre})$ and $I_{FRAP}(\text{pre})$ were calculated as the mean of 50 values of $I_{tot}(t)$ and $I_{FRAP}(t)$ before bleaching. These calculations were done in Microsoft Excel. For each condition, at least 20 acquisitions were done in two different experiments. The curves corresponding to the mean $I(t)$ value, as well as the 99% confidence interval, are shown on the graphs. The estimates of the mobile fractions were also calculated according to an alternative normalization as described in the figure legend to Fig. S3 in the supplemental material, which allows a direct reading of the mobile fraction and the standard errors. In order to get a better average value, the estimates correspond to the mean of the last 15 values of all experiments (t = 82.01 s to 88.22 s) and are within a 99% confidence interval (these values were not significantly different from those observed between t = 75.35 s and t = 81.56 s [data not shown]).

For FRAP experiments on cells in S phase, a control was carried out to check that cells were in S phase. During the FRAP experiment, the coordinates of the treated cells were noted. After the completion of the FRAP experiments, the cells were subjected to anti-CAF-1p150 immunofluorescence staining, the treated cells were observed, and only the FRAP data for cells with replication foci were analyzed.

For salt extraction experiments, the cells were grown on Bioptechs ΔT glass dishes and treated with increasing salt concentrations on the stage of a fully automatic Leica DMIRE2 microscope. First, the cells were washed with PB buffer (see "Immunoprecipitations, SDS-PAGE, and Western blotting" above), several representative fields were selected, and their positions were recorded by using Metamorph (Roper Scientific). Images of all the fields were acquired with a 40×, N Plan, NA0.55 CORR objective. PB buffer was replaced by PB buffer containing 0.2% Triton X-100 and 0.75 M NaCl, and images of the same fields were acquired with identical exposure times. The extraction buffer was then replaced by PB buffer containing 0.2% Triton X-100 and 2 M NaCl, and images of the same fields were acquired with identical exposure times. NaCl at a concentration of 0.75 M extracted H3-FP that was not deposited into chromatin, whereas 2 M NaCl extracted chromatin-bound H3-FP but did not extract H3-FP found in bright fluorescent nucleoli for the minority of transiently transfected cells that expressed aberrantly large amounts of H3-FP (see Fig. S1A in the supplemental material). This observation supports the idea that this population represents a sequestered population of hydrophobically aggregated H3-FP molecules. For all image acquisitions, the focal plane with maximal intensity was selected to correct for the possible focus drift due to changes in the media. The total fluorescence of single nuclei before and after extraction was determined after subtraction of local background noise, and fluorescence at 0.75 and 2 M was expressed as a percentage of the initial fluorescence. The values are within a 99% confidence interval. For Fig. 4E, the minimum and maximum gray values displayed were set identically for all images. As some cells never enter S phase after synchronization, the extent of H3.1WT remaining after 0.75 M salt extraction was assessed for H3.1WT-transfected cells that did not have S-phase foci and found to be lower than 25%. We kept only the cells where more than 25% of the fluorescence remained after extraction in 750 mM NaCl in order to ensure that we were analyzing cells in S phase.

RESULTS

hASF1 interaction with H3 involves H3 C-terminal arginines. To characterize the interaction between histones H3.1 and H3.3 with ASF1A and ASF1B in HeLa cells, we used histones H3.1 and H3.3 bearing a tag at their C termini. Similar constructs have already been abundantly characterized by others and shown to be active in vivo. Indeed, Kimura and Cook have shown that histone H3.1 tagged at its C terminus with GFP is incorporated into nucleosomes and behaves like endogenous histones (22). Tagami et al. have recently characterized C-terminal Flag-hemagglutinin-tagged histones H3.1 and H3.3 stably expressed in human cells (54); these histones were assembled into nucleosomes and present on chromosomes in mitosis. Here, we expressed histones H3.1 and H3.3 fused at their C termini with the Flag tag or fluorescent proteins (CFP, EGFP, enhanced yellow fluorescent protein, or the Venus variant of yellow fluorescent protein [36]) by transient transfection in HeLa cells. Transient transfection of tagged histones was previously used to study the dynamics of H3 assembly into chromatin (30, 42). As expected for transient transfections, the expression levels of H3-Venus varied from cell to cell (see Fig. S1 in the supplemental material). Moreover, a variable fraction of the cells exhibited an aberrant nucleolar concentration of the fluorescent histones that was often associated with highly fluorescent cells (see Fig. S1A and B in the supplemental material). The apparently excessive levels of H3-FPs in these cells may have contributed to their possible aggregation and sequestration in the nucleolus as has been reported for other GFP fusion constructs (40). For all our single-cell imaging, we avoided cells with fluorescent nucleoli and analyzed only cells showing a normal nucleoplasmic localization of H3-FPs. In those cells, we estimated the amount of tagged H3 to be at approximately 40% the amount of soluble endogenous H3 in an asynchronous population (see Fig. S2 in the supplemental material).

Endogenous ASF1A and ASF1B coimmunoprecipitated with transiently expressed H3.1-FP and H3.3-FP, as illustrated in Fig. 1A, lane 2, and Fig. 1B, lanes 2 and 3. In order to further analyze these interactions in vivo, we turned to the BiFC assay, where the two putative partners are fused to the first 172 amino acids or to the last 83 amino acids of CFP. If the two parts of CFP stay in close proximity, they form a functional fluorescent protein. Fluorescence thus indicates that the two putative partners interact (19). In our assay, where the transfection efficiency was about 70%, we detected the interaction of wild-type ASF1A with wild-type H3.1 in 60 to 70% of the cells (Fig. 1C and D). In contrast, using a V94R mutant of ASF1A and wild-type H3.1, fluorescence was seen in less than 7% of the cells. We showed previously that the ASF1-V94R mutation abolishes the ASF1-H3 interaction (32), and recent structural studies explain the disruptive effect of this mutation (2, 4, 10, 38). The BiFC assay thus faithfully reflects the in vivo interaction of ASF1A and H3.1.

We next set out to identify residues of H3 involved in the

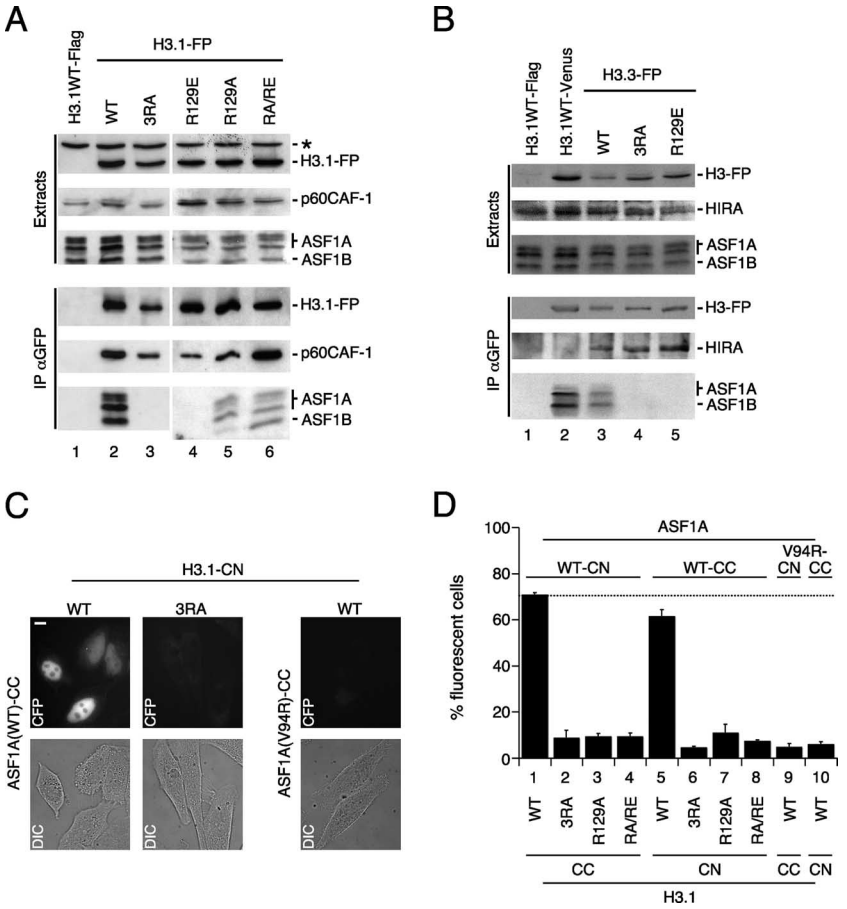

FIG. 1. Interaction of histone chaperones with wild-type (WT) and mutant H3 histones. (A and B) GFP fusion proteins were immunoprecipitated with anti-GFP antibodies (αGFP) 24 h after transfection of HeLa cells with the indicated constructs. Western blotting with anti-GFP, anti-p60CAF-1, anti-HIRA, or anti-hASF1 antibodies was carried out to assess the presence of these proteins before (Extracts) and after immunoprecipitation (IP αGFP). (A) Coimmunoprecipitation of p60CAF-1 and hASF1 with H3.1. Lane 1, H3.1WT-Flag; lane 2, H3.1WT-Venus; lane 3, H3.1-3RA-Venus; lane 4, H3.1R129E-CFP; lane 5, H3.1R129A-CFP; lane 6, H3.1RA/RE-CFP. The position of a nonspecific band revealed with anti-GFP antibodies is indicated by an asterisk to the right of the gel. Note that three bands corresponding to diversely phosphorylated ASF1A can be seen, as previously reported (50). Note also that there is no coimmunoprecipitation of hASF1 with H3.1-3RA and H3.1R129E, whereas coimmunoprecipitation of p60CAF-1 is retained. (B) Coimmunoprecipitation of HIRA and hASF1 with H3.3. Lane 1, H3.1WT-Flag; lane 2, H3.1WT-Venus; lane 3, H3.3WT-Venus; lane 4, H3.3-3RA-Venus; lane 5, H3.1R129E-CFP. Note that there is no coimmunoprecipitation of hASF1 with H3.3-3RA and H3.3R129E, whereas coimmunoprecipitation of HIRA is retained. (C) BiFC with ASF1A and H3.1. CFP autofluorescence images of HeLa cells transiently expressing H3.1 (WT or 3RA mutant) fused to residues 1 to 172 of CFP (CN) and ASF1A (WT or V94R mutant) fused to residues 155 to 238 of CFP (CC) 24 h after transfection (CFP fluorescence [CFP] or differential interference contrast [DIC]). The maximum and minimum levels of CFP fluorescence were adjusted to the same values for each of the images. Note the difference between cells with reconstituted CFP fluorescence in the nucleus (top left panel) and the faint cytoplasmic autofluorescence of cells transfected with either H3.1WT/ASF1A-V94R (top right panel) or H3.1-3RA/ASF1A-WT (top middle panel). Bar = 10 μm. (D) Quantification of BiFC efficiency for H3.1 mutants versus ASF1A. The percentage of cells exhibiting CFP fluorescence as exemplified in Fig. 1C was estimated in two separate experiments with all protein couples indicated under the histogram: $n = 211$ (bar 1), $n = 210$ (bar 2), $n = 196$ (bar 3), $n = 224$ (bar 4), $n = 232$ (bar 5), $n = 231$ (bar 6), $n = 201$ (bar 7), $n = 250$ (bar 8), $n = 196$ (bar 9), and $n = 177$ (bar 10). The mean values plus standard deviations (error bars) are shown. The average transfection efficiency in these experiments was estimated with an H3.1-CFP reporter construct and is represented here as a dotted line.

interaction with hASF1. ASF1A and ASF1B are histone H3/H4 chaperones, and the assembly of nucleosomes begins with the deposition of two H3/H4 dimers. We thus assumed that we could identify these residues by searching for regions of H3 that are accessible to interaction with a chaperone in the $(H3/H4)_2$/DNA subnucleosomal particle structure (extracted from the nucleosomal structure [28]). Additionally, we restricted our analysis to the last 39 residues of histone H3.1 (strictly conserved in H3.3), as they had already been shown to interact with ASF1A in a two-hybrid assay (34). Arginines 128, 129, and 134 of H3 fulfilled our criteria and could possibly participate in both electrostatic and hydrophobic interactions. Furthermore, these residues are found in the C-terminal 13 amino acids of H3 that interacted with ASF1 as determined by nuclear magnetic resonance analysis (32). These residues are also not involved in the H3/H3 interface and do not participate in the interaction with H4 (see Discussion).

We mutated R128, R129, and R134 and assessed the ability of the resulting H3 mutants to interact with ASF1A and ASF1B. All tagged mutants were expressed at levels similar to

those of the tagged wild-type protein in transient-transfection experiments (Fig. 1A and B) (see Fig. S1C and D in the supplemental material). As illustrated in Fig. 1A, lanes 3 and 4, and Fig. 1B, lanes 4 and 5, the triple mutation of R128, R129, and R134 to alanine (3RA), as well as the single mutation of R129 to glutamate (R129E) completely abolished interaction of either H3.1 or H3.3 with ASF1A and ASF1B in our coimmunoprecipitation assay. The 3RA mutation also abolished interaction of H3.1 with ASF1A in vivo in the BiFC assay (Fig. 1C and D). A single mutation of R129 to alanine or a double mutation of R128 to alanine and R134 to glutamate (RA/RE) resulted in a dramatically reduced interaction of H3.1 with ASF1A and ASF1B (Fig. 1A, lanes 5 and 6). We estimate that these mutants coimmunoprecipitated less than 5% of the ASF1A and ASF1B proteins coimmunoprecipitated with the wild type (data not shown). Interestingly, no interaction between ASF1A and these mutants could be detected in vivo in the BiFC assay, suggesting that this assay, albeit providing important information about in vivo interactions, is less sensitive in detecting residual interaction than the coimmunoprecipitation assay. Importantly, the 3RA, R129E, R129A, and RA/RE mutants of H3.1 maintained their interaction with p60CAF-1 (Fig. 1A), and the 3RA and R129E mutations did not affect the ability of H3.3 to interact with HIRA (Fig. 1B). We conclude from these data that the C-terminal arginine 129 and at least one of the two arginines (arginine 128 and 134) of H3 are involved in the interaction of tagged H3 with hASF1 but are not required for the interaction with p60CAF-1 and HIRA. These results prompted us to analyze the consequences of these mutations for the assembly of histones into nucleosomes.

Histone H3.1 mutants defective in ASF1 binding are diffusely distributed in the nucleoplasm during S phase. We first set out to compare the localization of newly synthesized wild-type and mutant histones during the S phase. Kimura and Cook showed that in heterokaryons formed between wild-type HeLa (nonfluorescent nuclei) and HeLa cells expressing H3.1-GFP (fluorescent nuclei), newly synthesized H3.1-GFP imported into nonfluorescent S-phase nuclei colocalized with "replication factories" (22). Replication factories are nuclear structures where DNA replication occurs. They were identified in the nuclei of mammalian cells as foci where analogues of nucleotides (e.g., BrdU) and proteins associated with the replication fork (e.g., PCNA) are detected by immunofluorescence microscopy (5, 31, 37). CAF-1, which interacts with PCNA, is also present in the replication factories (23). The apparent size, number, and localization of replication foci are different in early, mid, and late S phase. To confirm that newly synthesized H3.1-Venus was indeed present in replication foci in transiently transfected HeLa cells, we analyzed its localization 5 h after transfection. A small fraction of the transfected cells were already in or entered S phase during the incubation. As illustrated in Fig. 2A, H3.1-Venus was present in the replication factories identified by anti-p150CAF-1 immunofluorescence microscopy in patterns corresponding to early, mid, and late S phase. The foci seen with the anti-p150CAF-1 and the anti-GFP antibodies colocalized to a large extent as expected.

In order to analyze a large number of S-phase cells, we synchronized the cells with nocodazole and thymidine. The cells were transfected with the tagged histone constructs. The localization of the tagged proteins was assessed by immunofluorescence microscopy after the cells were released into S phase. We performed dual immunofluorescence labeling with anti-GFP and anti-BrdU antibodies in cells that had been released for 1 hour (Fig. 2B) or 2 hours (Fig. 2C) into S phase and where BrdU had been added to the culture medium at 37°C for 10 min before fixation. Under these experimental conditions, H3.1-Venus staining corresponds to the localization of tagged H3.1 that was synthesized during the synchronization protocol and after release into S phase, whereas the foci revealed with the anti-BrdU antibodies correspond to sites where DNA replication is taking place at the time of fixation. As illustrated in the blown-up area of the nucleus in Fig. 2B, one hour after the start of S phase, there is either colocalization or a good overlap between H3.1-Venus staining and the replication foci. In contrast, 2 hours after the start of S phase, H3.1-Venus staining showed only partial overlap with the replication foci (Fig. 2C). We interpret this first by the fact that the ratio of tagged H3.1 to endogenous H3.1 will be higher in very early S phase than later, thus making regions where chromatin has been assembled early in S phase potentially containing more label than at later times. Second, most of the assembled chromatin containing tagged H3.1 may simply have moved away from the actual sites of BrdU incorporation.

Since there was some disjunction between the replication foci and the tagged histone localization in synchronized cells, we decided to directly compare the localization of wild-type and mutant histones. We simultaneously transfected cells with one construct expressing wild-type H3.1-Flag and another expressing mutant H3.1-Venus and visualized their localization by dual anti-Flag and anti-GFP immunofluorescence. The localization of the tagged proteins was assessed by immunofluorescence microscopy 90 min after the cells were released into S phase. As illustrated in Fig. 3A, H3.1WT-Flag and H3.1WT-Venus were highly colocalized. In contrast, H3.1-3RA-Venus was more diffusely distributed in the nucleus and therefore did not colocalize well with H3.1WT-Flag. We also performed dual immunofluorescence labeling as described above on synchronized cells transfected with H3.1-3RA-Venus. As shown in Fig. 3C and D, at both 1 and 2 hours into S phase, H3.1-3RA-Venus staining was more diffuse and not clearly colocalizing with or adjacent to the replication foci (see Discussion).

We quantified the number of synchronized S-phase cells where the H3.1-Venus proteins precisely colocalized with H3.1WT-Flag (Fig. 3A, left column) versus cells where the localization of H3.1-Venus was diffuse (Fig. 3A, right column). The H3.1-3RA and H3.1R129E mutants colocalized with H3.1WT in 5.6% ± 2% and 4.4% ± 1% of the cells, respectively, whereas the H3.1R129A and H3.1RA/RE mutants colocalized with H3.1WT in 43% ± 5% and 20% ± 6% of the cells, respectively (Fig. 3B). Interestingly, H3.1R129A and H3.1RA/RE conserved a weak but detectable interaction with ASF1A and ASF1B (Fig. 1A and data not shown). The localization of H3.1 mutants in the foci revealed by wild-type H3.1 was thus in excellent correlation with their ability to interact with ASF1A and ASF1B.

Newly synthesized histone H3.1 and H3.3 deposition in chromatin during S and G_1 phases. We further characterized our H3 mutants using FRAP to assess the intranuclear mobile fraction

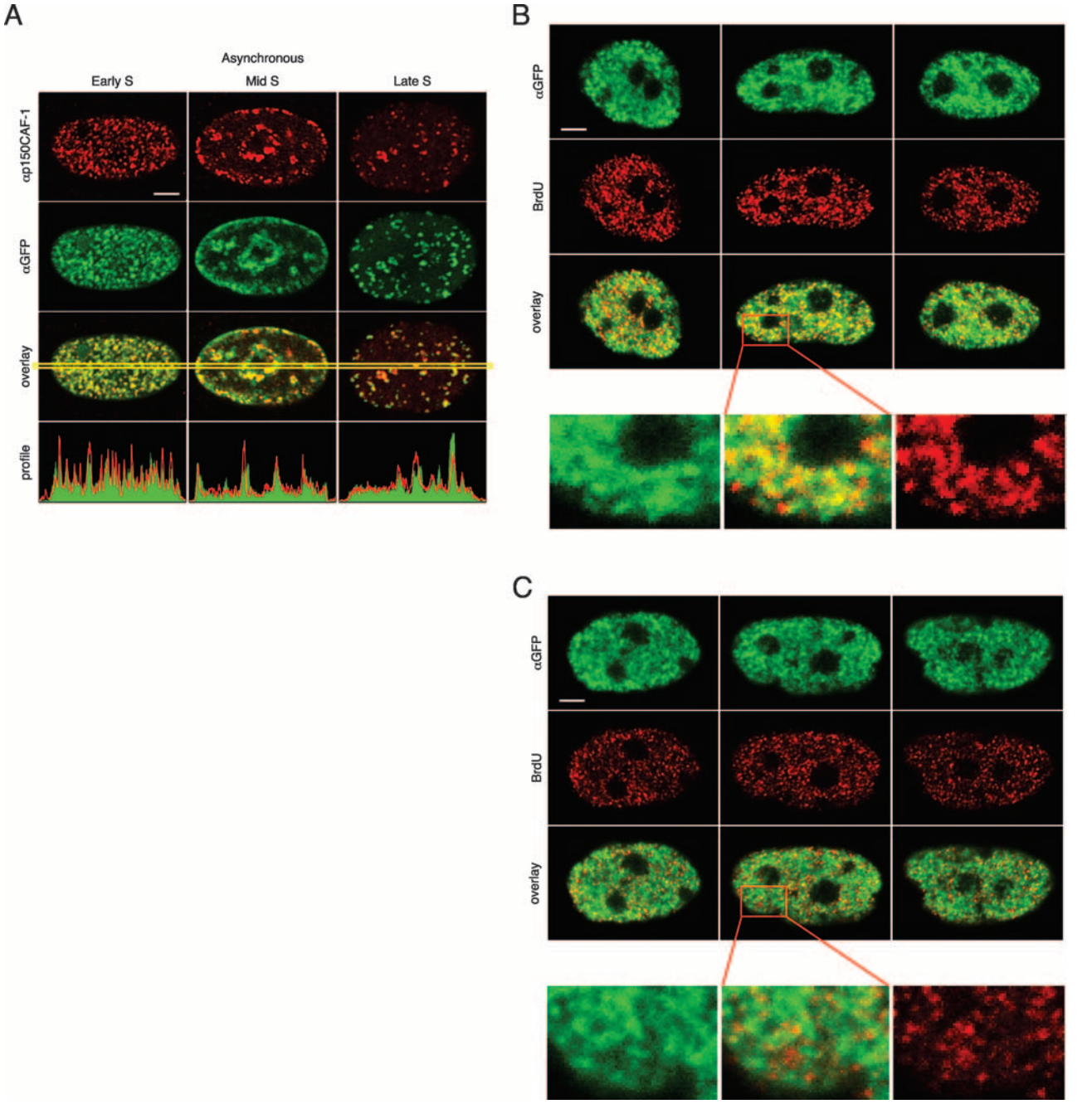

FIG. 2. Localization of newly synthesized wild-type H3.1 in S-phase cells. (A) Newly synthesized H3.1 is localized in replication foci in S-phase cells. Replication foci were revealed with anti-p150CAF-1 antibodies (αp150CAF-1) (red) in asynchronous HeLa cells. Transiently transfected H3.1-Venus was revealed with anti-GFP antibodies (αGFP) (green). The extent of colocalization can be estimated from the "overlay" panels and from the "profile" curves, which correspond to the intensity profiles in red and green along a line inside the yellow frame shown on the "overlay" panels. (B and C) Replication foci were revealed with anti-BrdU antibodies (red) in synchronized HeLa cells transiently transfected with H3.1WT-Venus, revealed with anti-GFP antibodies (green). Three typical nuclei are shown. The unlabeled bottom row of panels was taken with 3.6× zoom, corresponding to the red box on the overlap image. Cells were fixed 1 h (B) or 2 h (C) after release from the thymidine block. Bar = 5 μm.

of tagged histones. FRAP has previously been used in several studies of histone dynamics in animal cells. We reasoned that any difference in the assembly of the H3.1 mutants into nucleosomes would have consequences on the fraction of mobile histones. Indeed, Kimura and Cook have shown qualitative differences in the mobile fractions of H4-GFP in S-phase and non-S-phase nuclei (22). Additionally, while this study was being performed, Meshorer et al. described the use of FRAP to assess the mobile fraction of newly assembled histone H3 (30).

First, we confirmed that we could actually measure the difference of mobile fractions between assembled and unas-

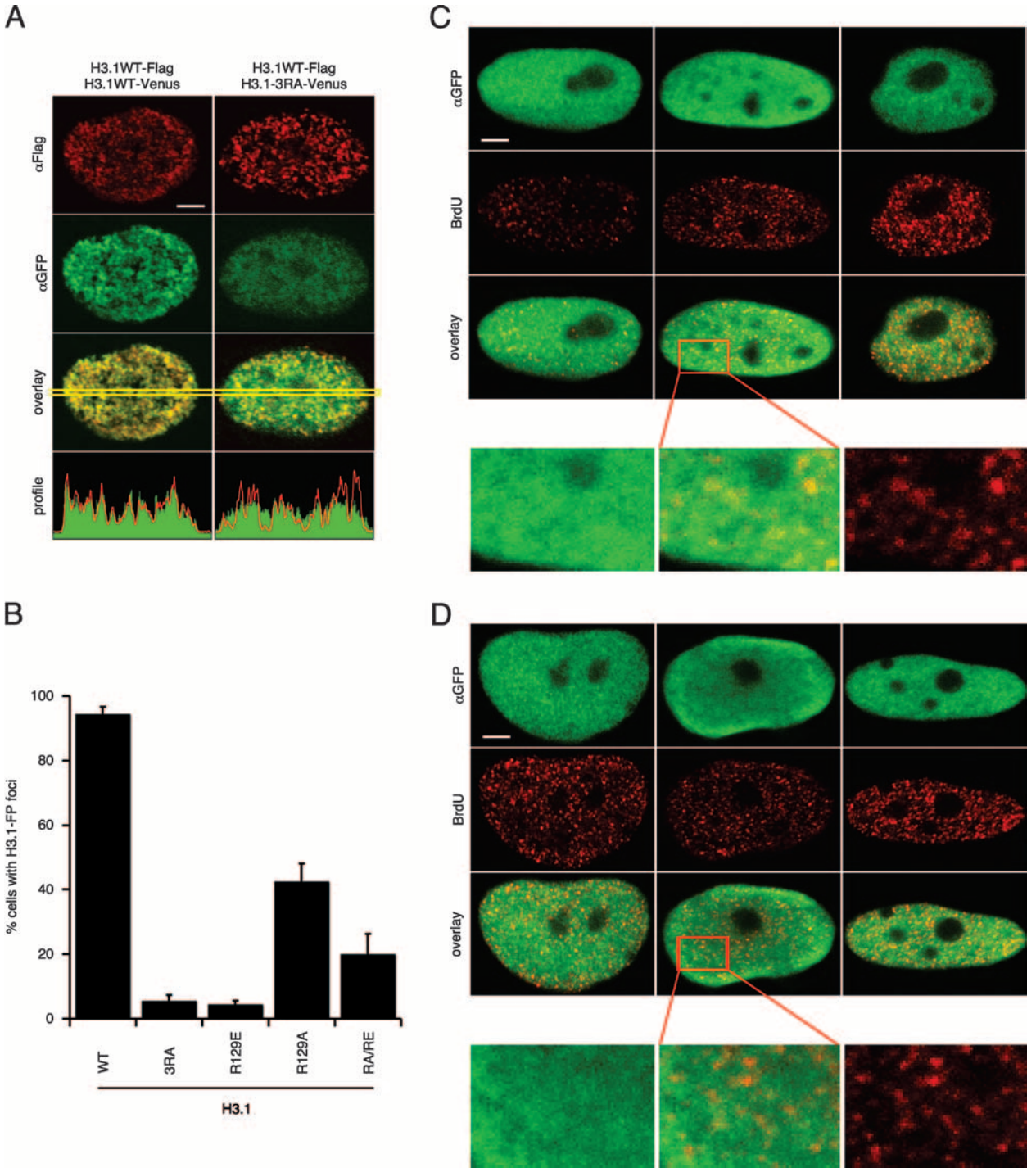

FIG. 3. Localization of newly synthesized mutant H3.1 in S-phase cells. (A) Localization of H3.1-3RA versus H3.1WT in synchronized S-phase cells. Replication foci were revealed with anti-Flag antibodies (αFlag) (red) in synchronized HeLa cells transiently transfected with H3.1WT-Flag, 1.5 h after release from a thymidine block. Cotransfected H3.1-Venus was revealed with anti-GFP antibodies (αGFP) (green). Note the colocalization between H3.1WT-Flag and H3.1WT-Venus in the panels on the left. Note the diffuse nuclear localization of H3.1-3RA-Venus and the diminished colocalization with H3.1WT in the panels on the right. Bar = 5 μm. (B) Quantification of the localization defects of H3.1 mutants. The histogram shows the percentage of cells in which the foci of H3.1-Venus (wild type [WT] or mutant as indicated) were clearly visible and colocalized with H3.1WT-Flag foci; the foci were observed by using anti-Flag and anti-GFP antibodies on synchronized S-phase HeLa cells transfected with H3.1WT-Flag and H3.1-Venus (WT or mutant). The presence of foci was assessed in at least five independent experiments on 642 (WT), 646 (3RA), 526 (R129E), 514 (R129A), and 672 (RA/RE) cells. The mean values plus standard deviations (error bars) are shown. (C and D) Replication foci were revealed with anti-BrdU antibodies (red) in synchronized HeLa cells transiently transfected with H3.1-3RA-Venus or revealed with anti-GFP antibodies (green). The unlabeled bottom row of panels was taken with 3.6× zoom, corresponding to the red box on the overlap image. Three typical nuclei are shown. Cells were fixed 1 h (C) or 2 h (D) after release from the thymidine block. Bar = 5 μm.

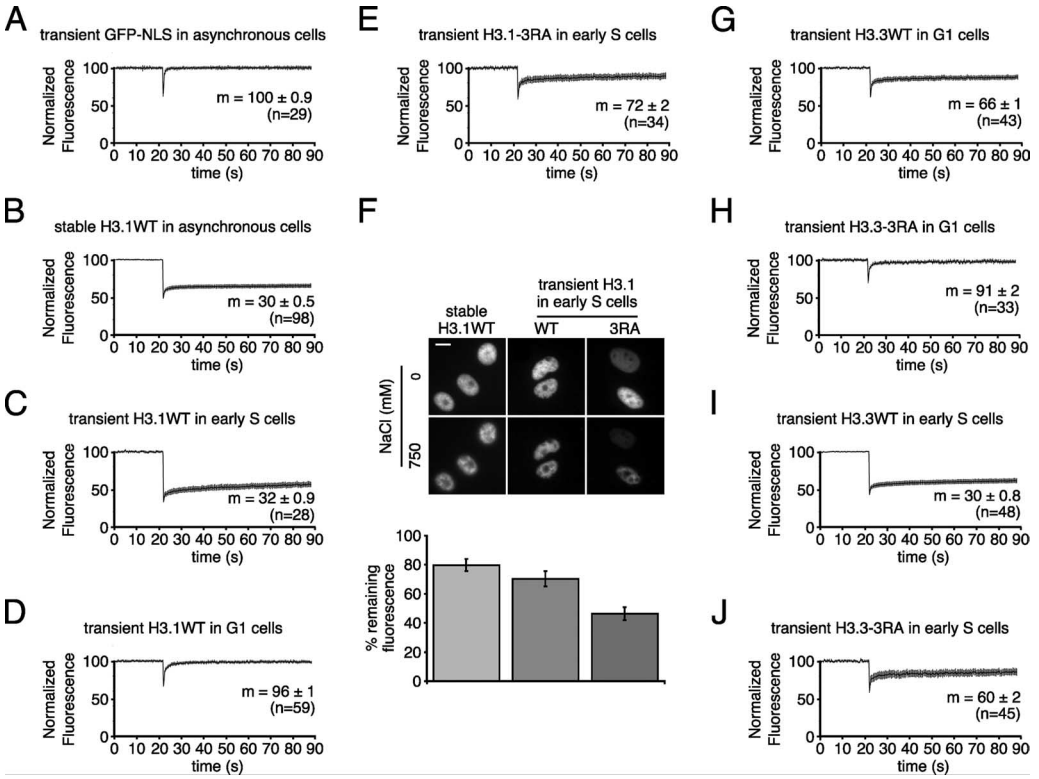

FIG. 4. Deposition of newly synthesized histone H3.1 and H3.3 in chromatin during S and G_1 phases. (A to E and G to J) Normalized fluorescence (arbitrary units) recovered after photobleaching in HeLa cells. The curve (black) represents the mean of *n* distinct acquisitions after normalization. The vertical bars along the curves represent the 99% confidence interval. The average values (*m*) correspond to the mean of the last 15 fluorescence values for all *n* acquisitions (±99% confidence interval [see Materials and Methods for calculation method]). (A) Asynchronous cells expressing the GFP nuclear localization signal (GFP-NLS). GFP-NLS was exclusively nuclear. (B) Asynchronous cells stably expressing H3.1WT-GFP. (C) Synchronized S-phase cells transiently expressing H3.1WT-Venus. (D) Synchronized G_1-phase cells transiently expressing H3.1WT-Venus. (E) Synchronized S-phase cells transiently expressing H3.1-3RA-Venus. (G) Synchronized G_1-phase cells transiently expressing H3.3WT-Venus. (H) Synchronized G_1-phase cells transiently expressing H3.3-3RA-Venus. (I) Synchronized S-phase cells transiently expressing H3.3WT-Venus. (J) Synchronized S-phase cells transiently expressing H3.3-3RA-Venus. As expected, there is a correlation between the extent of photobleaching and the fraction of rapidly diffusing, mobile protein (41). (F) Percentage of fluorescence intensity remaining in the nuclei after salt extraction. Cells stably expressing H3.1WT-GFP were asynchronous. Transiently transfected HeLa cells were synchronized in early S phase (1 to 2 h after release from thymidine block). The cells were treated successively with 0 mM and 750 mM NaCl. (Top) Nuclei before (0 mM NaCl) and after (750 mM NaCl) salt extraction. Not all nuclei retained their shape after extraction (not shown). Bar = 10 μm. (Bottom) Quantification of the remaining fluorescence after salt extraction, expressed as a percentage of fluorescence in 0 mM NaCl (with 99% confidence interval). The data shown correspond to two independent extractions on 68 cells (stably expressing H3.1WT), 63 cells (transiently expressing H3.1WT), and 58 cells (transiently expressing H3.1-3RA).

sembled proteins. FRAP was carried out on a rectangular region of the nucleus representing less than 5% of the nuclear surface in the focal plane. All the results presented here correspond to the analysis of at least 20 cells from two different experiments. The fluorescence recovery values for all experiments were normalized, which allowed a statistical analysis of the results and a direct estimation of the mobile and immobile fractions. Using this protocol, 100% ± 0.9% of GFP fused to a nuclear localization signal was mobile ($n = 29$) (Fig. 4A) (see Fig. S3A in the supplemental material). In contrast, only 30% ± 0.5% of H3.1WT-EGFP in HeLa cells stably expressing the protein was mobile ($n = 98$) (Fig. 4B) (see Fig. S3B in the supplemental material). We synchronized cells as previously described and found that 32% ± 0.9% of newly synthesized H3.1WT-Venus after 1.5 h into S phase was mobile ($n = 28$) (Fig. 4C) (see Fig. S3C in the supplemental material). These results are consistent with those of Meshorer et al. (30) and Kimura and Cook (22).

We next analyzed the fraction of H3.1 that is mobile under conditions where it is not normally assembled, i.e., outside of S phase. We synchronized HeLa cells by mitotic shake-off as described above and found that 96% ± 1% of H3.1 was mobile after 7 h into G_1 phase ($n = 59$) (Fig. 4D) (see Fig. S3D in the supplemental material). This demonstrated that when it is not incorporated, wild-type H3.1 is almost entirely mobile in the nucleoplasm. We then measured the fraction of H3.1-3RA-Venus that is mobile in S phase. Cells were synchronized and transfected as described above, and 72% ± 2% of H3.1-3RA-Venus was mobile ($n = 34$), which is much greater than the percentage of H3.1WT-Venus that was mobile (Fig. 4E) (see Fig. S3C in the supplemental material).

The changes in mobile fractions could result from differences in chromatin assembly but also from differences in interactions with macromolecular complexes in the nucleus. To check whether macromolecular interactions distinct from assembly in nucleosomes could play a significant part in the

extent of changes between the wild-type histones and the mutant histones, we performed salt extraction on cells synchronized and transfected as for the FRAP experiments. Whereas the soluble nuclear proteins and some of the nucleosomal H2A and H2B are extracted from chromatin with 750 mM NaCl, nucleosomal histones H3 and H4 are resistant to extraction at this salt concentration, but they are extracted at 2 M NaCl (22, 53). Indeed, for wild-type H3.1-EGFP stably expressed in HeLa cells, about 20% of the fluorescence was extracted with 750 mM NaCl in asynchronous cells (Fig. 4F), and the remainder was subsequently extracted with 2 M NaCl (not shown). We also measured about 20% soluble fluorescent H3.1 by Western blotting with anti-GFP antibodies (see Fig. S2C in the supplemental material). As shown in Fig. 4F, about 30% of wild-type fluorescent H3.1 was extracted from early S-phase nuclei with 750 mM NaCl (all H3.1WT was subsequently extracted with 2 M NaCl [not shown]). This showed that 70% of newly assembled wild-type H3.1 behaved as nucleosomal histone H3. Interestingly, as shown in Fig. 4F, more than 50% of the H3.1-3RA-Venus fluorescence was extracted from early S-phase nuclei with 750 mM NaCl (all H3.1-3RA was subsequently extracted with 2 M NaCl [not shown]). We conclude from this experiment that about 46% of H3.1-3RA is assembled in nucleosomes under these experimental conditions, though this mutant does not interact with hASF1 and does not colocaliz well with replication foci.

Importantly, the salt-resistant H3 fraction was comparable to the immobile fraction observed in the FRAP experiments, which confirmed that the immobile fraction indeed corresponds to the fraction of H3-FP incorporated into chromatin. Since the cells are kept alive and under culture conditions during the FRAP experiments, they are more likely to reveal physiological differences in the assembly of histones in chromatin. All further experiments were carried out using exactly the same FRAP protocol.

We then analyzed the mobile fractions of WT and mutant histone H3.3-Venus. Wild-type H3.3 is assembled into nucleosomes by SI assembly pathways that are active both inside and outside of the S phase. We synchronized HeLa cells in G_1 as described above and found that 66% ± 1% of H3.3WT-Venus was mobile after 7 h in G_1 (n = 43) (Fig. 4G) (see Fig. S3E in the supplemental material). This confirmed, in comparison with the mobile fraction of H3.1, that H3.3 is incorporated into chromatin outside of S phase. Interestingly, 91% ± 2% of H3.3-3RA-Venus was mobile after 7 h in G_1 (n = 33) (Fig. 4H) (see Fig. S3E in the supplemental material), which is thus significantly more mobile than H3.3WT-Venus, showing that the H3.3-3RA mutant is defective for assembly during G_1. We also found that 30% ± 0.8% of newly synthesized H3.3WT was mobile in early S phase in cells synchronized as described above for H3.1 (n = 48) (Fig. 4I) (see Fig. S3F in the supplemental material). The mobile fractions of wild-type H3.1 and H3.3 in early S phase are thus similar. Note that, under our experimental conditions, H3.3 was expressed in synchronized cells for 17 h before release into S phase and was therefore also assembled into chromatin in G_1 by replication-independent mechanisms. In comparison, 60% ± 2% of H3.3-3RA-Venus was mobile in S phase (n = 45) (Fig. 4J) (see Fig. S3F in the supplemental material), showing that the H3.3-3RA mutant is also defective for assembly during S phase.

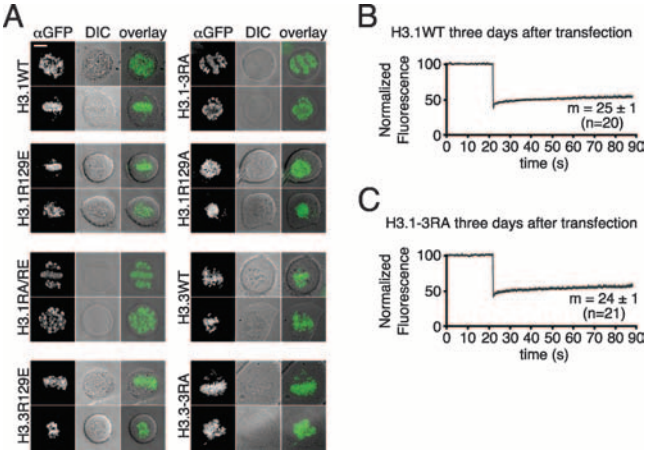

FIG. 5. Mutant H3 histones unable to bind hASF1 end up in chromatin. (A) HeLa cells were transfected with the indicated constructs (H3.1WT-Venus, H3.1-3RA-Venus, H3.1R129E-CFP, H3.1R129A-CFP, H3.1RA/RE-Venus, H3.3WT-Venus, H3.3R129E-CFP, and H3.3-3RA-Venus). Three days after transfection, the cells were treated with nocodazole for 5 h in order to enrich the population in mitotic cells and then treated for immunofluorescence with anti-GFP antibodies (αGFP). DIC, differential interference contrast. Note that H3-FP is detected only on the chromosomes for all the constructs. Note also that atypical mitotic figures are due to the nocodazole treatment. Bar = 10 μm. (B and C) Normalized fluorescence (arbitrary units) recovered after photobleaching in HeLa cells 3 days after transfection. The curve (black) represents the mean of n distinct acquisitions after normalization. The vertical bars along the curves represent the 99% confidence interval. The average values (m) correspond to the mean of the last 15 fluorescence values for all n acquisitions (±99% confidence interval). (B) H3.1WT-Venus; (C) H3.1-3RA-Venus.

In addition to the results of the salt extraction experiment, we also obtained independent confirmation that the H3.1-3RA mutant was assembled into chromatin. First, when we analyzed the localization of the H3.1 mutants at 3 days posttransfection, we observed that the H3.1 mutants were all present on mitotic chromosomes (Fig. 5A). Second, we performed FRAP analysis on asynchronous interphase cells 3 days after transfection and compared the results to those of the mobile fractions of H3.1WT-Venus and H3.3WT-Venus under the same conditions. We obtained values of 25% ± 1% (n = 20), 24% ± 1% (n = 21), 23% ± 1% (n = 20), and 21% ± 0.9% (n = 22) for H3.1WT-Venus, H3.1-3RA-Venus, H3.3WT-Venus, and H3.3-3RA-Venus, respectively (Fig. 5B and C and data not shown). These values confirm the stable deposition of the mutant H3 histones into chromatin.

The lesser, but significant, incorporation of the mutants in early S phase (H3.1 and H3.3) and in G_1 (H3.3) appears sufficient to explain that the wild-type and mutant histones are indistinguishable in their chromatin deposition after long-term expression, although we cannot exclude other mechanisms. We conclude that the mutants of H3.1 and H3.3 that are defective in their interaction with ASF1A and ASF1B are incorporated into chromatin with slower kinetics compared to wild-type histones in early S phase (H3.1 and H3.3) and in G_1 (H3.3). Their inefficient integration into chromatin may involve ASF1-independent assembly pathways or weak in vivo residual interactions with ASF1A/B that allow inefficient chromatin deposition.

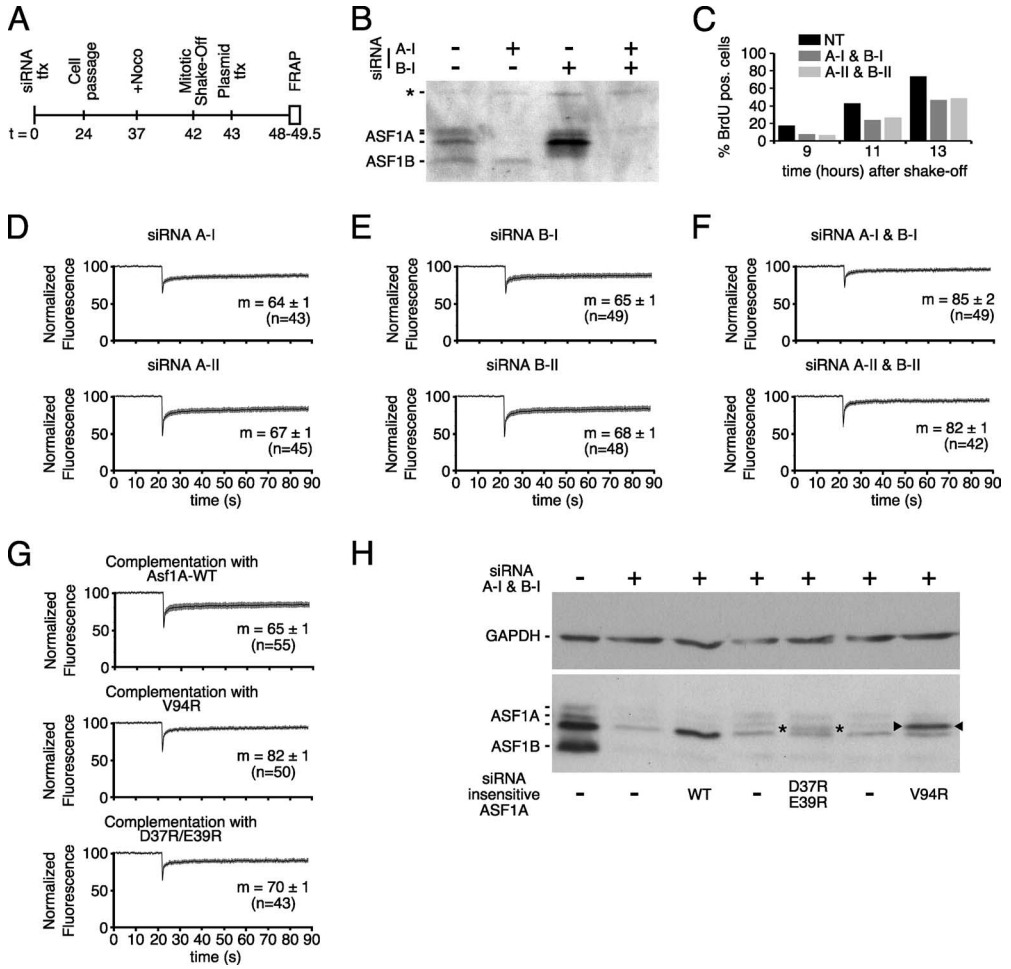

FIG. 6. Chromatin deposition of wild-type H3.3 in hASF1-depleted cells and complementation by wild-type and mutant ASF1A. (A) Experimental time line for HeLa cell transfection (tfx) with siRNA, synchronization, transfection with plasmids, and FRAP analysis. +Noco, treated with nocodazole. (B) Anti-hASF1 Western blot showing the extent of hASF1 knockdown by siRNA (as indicated) in extracts of cells harvested after FRAP experiments. The position of a nonspecific band revealed with anti-hASF1 antibodies is indicated by an asterisk to the left of the gel. (C) Measure of the length of G_1 phase in undepleted (not treated with siRNA [NT]) and hASF1-depleted synchronized cells. BrdU was added immediately after release from the mitotic block (shake-off). BrdU-positive (pos.) cells were counted after shake-off on 696, 813, and 503 cells (undepleted or not treated [NT]), 1,017, 748, and 757 cells (depleted with A-I and B-I), 669, 835, and 663 cells (depleted with A-II and B-II) after 9, 11, and 13 h, respectively. (D to G) Normalized fluorescence (arbitrary units) recovered after photobleaching in HeLa cells. The black curves represent the mean of *n* distinct acquisitions after normalization. The vertical bars along the curve represent the 99% confidence interval. The average values (*m*) correspond to the mean of the last 15 fluorescence values for all *n* acquisitions (±99% confidence interval). (D) HeLa cells treated with siRNA A-I or A-II. (E) HeLa cells treated with siRNA B-I or B-II. (F) HeLa cells treated with siRNA A-I and B-I or A-II and B-II. (G) HeLa cells treated with siRNA A-I and B-I and transfected with siRNA-insensitive ASF1A-WT (top panel), ASF1A-V94R (middle panel), or ASF1A-D37R+E39R (bottom panel). (H) Western blotting of hASF1-depleted HeLa cells with (+) or without (−) expression of siRNA-insensitive wild-type (WT) and mutant ASF1A as indicated. Extracts from cells treated identically to the cells in panel G, but not subjected to FRAP. The positions of ASF1A-D37R+E39R (asterisks) and ASF1A-V94R (▶) are indicated on the gels. An anti-glyceraldehyde-3-phosphate dehydrogenase (anti-GAPDH) Western blot on the same membrane is shown as a loading control.

Both ASF1A and ASF1B participate in H3.3 chromatin deposition in G_1 phase. The assembly defects of H3.1 and H3.3 mutants unable to interact with ASF1A/B suggested that their interaction with these chaperones was crucial for efficient assembly into chromatin. We further tested this idea by examining the effect of depleting ASF1A and/or ASF1B on the nucleosomal assembly of newly synthesized wild-type H3 histone. Simultaneous depletion of hASF1A and hASF1B causes cells to accumulate in S phase (14, 15, 47, 48). The dramatic S-phase block would make it difficult to distinguish direct from indirect effects of ASF1A/B depletion on the deposition of H3.1 in S phase. Therefore, we decided to concentrate on the effect of hASF1 depletion on the deposition of H3.3 in G_1-phase cells. We first determined the effect of hASF1 depletion on G_1-phase progression. We used two unrelated siRNAs for ASF1A (A-I and A-II) and ASF1B (B-I and B-II) for hASF1 knockdown. Cells were treated with siRNA and synchronized in mitosis as shown in Fig. 6A. The extent of hASF1 knockdown is shown in Fig. 6B. To analyze the consequences of hASF1 depletion on the duration of the G_1 phase, we added BrdU immediately after mitotic release to allow the detection of S-phase cells at the end of G_1. As shown in Fig. 6C, between 9

and 13 h after the release from the nocodazole block, we observed a linear accumulation of S-phase cells for depleted and undepleted cells. However, at all time points, there were more cells in S phase in the undepleted population than in the population depleted for hASF1. From these data, it can be deduced that about 14% of the undepleted cells enter S phase every hour compared with 10% for the cells depleted of hASF1. Interpolation to the origin suggested that the first undepleted cells started S phase about 8 h after the release from the nocodazole block compared with 8.5 h for the cells depleted of hASF1. It can be concluded that depletion of hASF1 results in a modest lengthening of G_1 phase.

We next examined the effect of hASF1 depletion on the mobile fraction of H3.3WT-Venus in G_1 phase. As shown in Fig. 6D and E, the fraction of H3.3WT-Venus that remains mobile in G_1-phase cells was not significantly different in cells depleted either for ASF1A or for ASF1B and in untreated cells (compare Fig. 4G, [66% ± 1%], Fig. 6D [A-I, 64% ± 1%; n = 43] [A-II, 67% ± 1%; n = 45], and Fig. 6E [B-I, 65% ± 1%]; n = 49] [B-II, 68% ± 1%; n = 48]) (also see Fig. S3G and H in the supplemental material). In contrast, in G_1-phase cells depleted for both ASF1A and ASF1B, the mobile fraction of H3.3WT-Venus was significantly higher (Fig. 6F) (see Fig. S3I in the supplemental material): 85% ± 2% (n = 49) for A-I and B-I and 82% ± 1% (n = 42) for A-II and B-II. The mobile fraction of H3.3WT-Venus in G_1 cells depleted for both ASF1A and ASF1B resembled the mobile fraction of H3.3-3RA-Venus in untreated G_1 cells (91% ± 2%) (Fig. 4H). These results suggested that G_1-phase cells depleted for both ASF1A and ASF1B have a defect in the assembly of newly synthesized H3.3 into chromatin.

Although the phenotypes observed after depletion of proteins with two different siRNAs are usually attributed to impaired function of those proteins, it remains formally possible that they are due to off-target effects of the siRNAs. We therefore set out to confirm that the increased mobile fraction of H3.3WT-Venus in G_1 cells depleted for hASF1 was indeed due to impairment of ASF1A and ASF1B function by restoring the expression of ASF1A. To this end, we first constructed an ASF1A-mCherry expression plasmid in which the ORF of ASF1A had been rendered insensitive to siRNA A-I by silent point mutations. Following the same experimental protocol, cells were depleted of hASF1 by siRNAs A-I and B-I, synchronized, and cotransfected with H3.3WT-Venus and ASF1A-mCherry constructs in a 1:2 ratio. This allowed for the identification of cells coexpressing both fusion proteins. All cells expressing H3.3WT-Venus were found to express ASF1A-mCherry to various extents (not shown). Surprisingly, when we performed FRAP experiments on those cells, we obtained two strikingly distinct populations: in the cells with a low level of ASF1A-mCherry fluorescence, where fluorescence was exclusively nuclear, the H3.3WT-Venus mobile fraction was 66% ± 3% (n = 14) (graph not shown), similar to what we observed for undepleted cells, and indicative of complementation of function by the ASF1A-mCherry construct. In contrast, in cells with a higher level of ASF1A-mCherry fluorescence, where fluorescence was both nuclear and cytoplasmic, the H3.3WT-Venus mobile fraction was 91% ± 2% (n = 13) (graph not shown), similar to what was observed for H3.3-3RA-Venus in undepleted cells. These results suggested that the overexpression of the ASF1A-mCherry fusion protein hindered ASF1A function. We were worried that the presence of mCherry itself could cause or aggravate the lack of complementation in cells expressing high levels of the fusion protein. Since we had observed that all cells expressing H3.3WT-Venus also expressed ASF1A-mCherry, we decided to introduce a stop codon between ASF1A and mCherry, so that the protein expressed after transfection of the construct was wild-type ASF1A only. As shown in Fig. 6G and in Fig. S3J in the supplemental material, using this construct and the same experimental conditions, a single-cell population was observed in the FRAP experiments, and the H3.3WT-Venus mobile fraction was 65% ± 1% (n = 55). Figure 6H shows the extent of hASF1 depletion and of wild-type ASF1A reexpression. This result strongly suggests that wild-type ASF1A is able to complement the depletion of both ASF1A and ASF1B for the incorporation of H3.3WT-Venus in chromatin in G_1 cells. To further confirm that this was due to a function of ASF1A linked to its interaction with histone H3, we performed the same experiment with the ASF1A-V94R mutant. Figure 6H shows the extent of ASF1A-V94R expression in hASF1-depleted cells. As shown in Fig. 6G and in Fig. S3K in the supplemental material, the mobile fraction in this assay was 82% ± 1% (n = 50), indicating that histone binding was required for ASF1A activity in G_1. The H3.3WT-Venus mobile fraction was 66% ± 2% (n = 25) (graph not shown) in undepleted G_1 HeLa cells where ASF1A-V94R was expressed, showing that ASF1A-V94R had no dominant-negative activity.

The ASF1A-HIRA interaction has been characterized, and several mutations that disrupt the ASF1A-HIRA interaction have been described. In particular, Daganzo et al. have shown that the ASF1A-H36R+D37R does not bind HIRA in vitro (8). Recently, Tang et al. carried out structural characterization of the HIRA-ASF1A interface and showed that the single D37A mutation was sufficient to disrupt interaction of ASF1A with a minimal interaction domain of HIRA in vitro and also showed that E39 was involved in the interaction (55). We have previously reported that the *S. cerevisiae* Asf1-D37R+E39R mutant has in vivo silencing defects but is still able to bind histone H3 (32). These phenotypes are most likely attributable to lack of Hir binding. Altogether, these results strongly suggest that the ASF1A-D37R+E39R mutant is unable to bind HIRA. We therefore decided to assay the complementation of hASF1 depletion by the ASF1A-D37R/E39R mutant. As shown in Fig. 6G and in Fig. S3K in the supplemental material, the mobile fraction of H3.3WT-Venus in cells reexpressing ASF1A-D37R+E39R (Fig. 6H) was 70% ± 1% (n = 43), showing that this mutant is able to complement hASF1 depletion, albeit slightly less efficiently than wild-type ASF1A (this may be due in part to lower expression of this mutant compared to the wild type [Fig. 6H]). This result strongly suggests that HIRA binding is not required for ASF1A function in H3.3 deposition in G_1 cells.

DISCUSSION

We studied the interaction between human histone H3 chaperones ASF1A and ASF1B and the major H3 isoforms, H3.1 and H3.3. We identified mutants of H3.1 and H3.3 that

are defective in their interaction with both hASF1 isoforms but are still competent to bind CAF-1 and HIRA, respectively. Remarkably, these H3.1 and H3.3 mutants are defective for their efficient assembly into nucleosomes. Finally, we showed that depletion of both ASF1A and ASF1B is required for impairment of DNA synthesis-independent assembly of wild-type H3.3 and that expression of wild-type ASF1A and ASF1A-D37R+E39R, but not ASF1A-V94R, could reverse this phenotype. These results highlight the role of hASF1 in nucleosome assembly in vivo, indicate a degree of redundancy in the actions of ASF1A and ASF1B, and suggest that HirA is not required for DNA synthesis-independent nucleosome assembly in human cells.

The hASF1-H3 interaction involves C-terminal arginines of H3. The C-terminal arginine 129 together with at least one of the two arginines (arginine 134 and 128) of H3 are involved in the interaction of tagged H3 with hASF1 (Fig. 1). These residues are located near the interface between the two H3 polypeptides in the nucleosome. However, they do not directly participate in the interface or in H4 binding, which are therefore unlikely to be affected. Indeed, even though H3-R129E and H3-3RA are not efficiently integrated into chromatin (Fig. 3 and 4), they are slowly deposited by less efficient deposition pathways in HeLa cells (Fig. 5). Had the mutations severely impaired the formation of the H3/H3 interface or of the H3/H4 dimer, we would have expected a measurable difference with the dynamic behavior of wild-type H3. Instead, we found that these mutants behaved dynamically like wild-type H3 once incorporated into chromatin (Fig. 4C and 5B and C), supporting the lack of an important role for these arginines in the stability of the assembled nucleosome.

Very recently, we and others published structures of the ASF1-H3 or ASF1-H3/H4 interfaces (2, 4, 10, 38). These structures showed an extensive interface between ASF1 and H3, and they revealed the structural basis for the binding of ASF1 to a heterodimeric complex of H3/H4. Interestingly, the structures clearly show an important electrostatic interaction between ASF1-D54 and H3-R129, whereas H3-R134 makes less important contributions to the interaction and H3-R128 is not involved. This is in complete accord with the results of our mutational analyses. Remarkably, the R129E and 3RA mutants of H3.1 and H3.3 still bind CAF-1 and HIRA, respectively. Thus, these chaperones must interact with histone H3 through a distinct binding mode that is presumably involved in the specific association of CAF-I with H3.1 and HirA with H3.3 (54).

Implication of hASF1 in nucleosome assembly in vivo. ASF1 has been implicated in both nucleosome assembly and disassembly (for a review, see reference 33). In vitro experiments have shown that ASF1 can synergize with CAF-1 and Hir proteins to facilitate SC and SI nucleosome assembly, respectively (13, 54). However, a recent study has shown that *Xenopus* ASF1 is dispensable for direct de novo histone deposition in either pathway in egg extracts (45). Furthermore, in vivo data supporting a nucleosome assembly role for ASF1 have been less clear. In budding yeast, the *asf1*Δ mutant is viable and does not appear to show major defects in nucleosome density (1, 44). In *Drosophila* and vertebrate cells, depletion of ASF1 slows progression through S phase, but the molecular basis of this inhibition is unknown (14, 15, 47, 48). Indeed, it was recently suggested that inhibition of replication fork progression in the absence of hASF1 could be due to inefficient dissociation of nucleosomes in front of the MCM helicase (14). Nevertheless, depletion of ASF1 in chicken DT-40 cells led to increased nuclease sensitivity of newly synthesized DNA, which is consistent with a role for ASF1 in DNA synthesis-coupled nucleosome assembly (47). In this work, we used fluorescence microscopy to study the roles of hASF1 isoforms in H3 deposition in HeLa cells. First, we showed that histone mutants unable to interact with hASF1 are not efficiently assembled into chromatin in vivo, even though they are still able to bind CAF-1 or HIRA. Second, we showed that simultaneous depletion of ASF1A and ASF1B prevented efficient DNA synthesis-independent assembly of wild-type H3.3-FP into chromatin. We did not determine the effect of ASF1A and ASF1B depletion on DNA synthesis-coupled deposition of H3.1 in S phase, because the known severe inhibition of S-phase progression in this condition would make it impossible to determine whether a defect of H3.1 assembly was a direct or indirect consequence of hASF1 depletion. We have also observed that depletion of hASF1 slightly slows progression through G_1 phase in synchronized cells. It thus remains formally possible that the lower chromatin deposition of H3.3 in these cells is an indirect result of the slower progression through G_1 phase. However, since the H3.3-3RA mutant is also deposited less efficiently and since the function of ASF1A in G_1 requires histone binding, the simplest hypothesis is that hASF1 depletion impairs histone deposition, which in itself might be responsible for a modest lengthening of the G_1 phase. Understanding the mechanisms of G_1-phase lengthening and the consequences of hASF1 depletion in S phase on histone deposition will be the subject of future enquiries. Nonetheless, our combined results provide the most direct evidence to date for an in vivo role of ASF1A and ASF1B in nucleosome assembly in human cells.

Nucleosome assembly pathways in human cells. We identified H3.1 and H3.3 mutants that are defective in hASF1 interaction but that retain binding to CAF-1 and HIRA, respectively. Interestingly, although these mutants are not efficiently assembled into chromatin by either the SC or SI assembly pathway, they are deposited slowly into chromatin and end up associated with mitotic chromosomes. These results suggest that hASF1 is required for efficient nucleosome assembly in human cells but that inefficient assembly pathways that function with little or no hASF1 may exist. This residual nucleosome assembly may be due to an inefficient activity of CAF-1 and HIRA in the absence of hASF1 in HeLa cells. In this model, hASF1 could be thought of as a processivity factor for efficient nucleosome assembly. Alternatively, CAF-1 and HIRA may be totally inactive for chromatin assembly of newly synthesized H3 in the absence of hASF1, in which case the residual deposition of H3 would be due to distinct histone chaperones that are only able to inefficiently assemble newly synthesized H3 into chromatin. Finally, we cannot exclude the possibility that some assembly of our ectopically expressed H3-fluorescent proteins is due to their constitutive expression. Further work is needed to distinguish between these possibilities.

Both ASF1A and ASF1B participate in DNA synthesis-independent assembly of histone H3.3 into chromatin. Current

models of SI assembly implicate a HIRA/ASF1A pathway that would not involve ASF1B. However, our data clearly show that depletion of both ASF1A and ASF1B is required to inhibit H3.3 deposition into G_1-phase chromatin. This indicates that ASF1A and ASF1B have redundant functions in SI assembly. This result contrasts with the unique role of ASF1A in SAHF formation in primary human fibroblasts, where depletion of ASF1A alone is sufficient to impair the formation of the SAHF (61). SAHF formation would in this respect be mechanistically different from nucleosome assembly in cycling G_1-phase cells. An interesting possibility is that both ASF1A and ASF1B are involved in SI nucleosome assembly in vivo in proliferating cells, whereas only ASF1A would be involved in nucleosome assembly/disassembly in quiescent or senescent cells. The evidence so far shows a strong preference of HIRA for ASF1A. Tang et al. have provided biochemical data showing that this specificity depends on the N-terminal and C-terminal regions of ASF1A that are less conserved in ASF1B (55). Our data suggest that HIRA binding is not required for the G_1 deposition of H3.3 that depends on ASF1A, which could explain why either ASF1A or ASF1B is sufficient for G_1 deposition of H3.3. Thus, even though hASF1 seems to be important in the efficiency of histone deposition in S phase as a processivity factor and/or a histone donor for CAF-1, it seems that its function in G_1 deposition of H3.3 is largely independent of HIRA. Whether hASF1 functions on its own as a bona fide histone deposition factor in G_1 cells or whether it acts through an as yet unidentified factor will be the subject for future investigations.

ACKNOWLEDGMENTS

We thank M. Blondel, K. Seeger, P. Baudouin-Cornu, and S. Chédin for critical reading of the manuscript and helpful comments and C. Carles for advice on the figures. J.-Y.T. acknowledges the support and encouragement of A. Sentenac. We also thank H. Sillje and E. Nigg for the kind gift of anti-hASF1 antibodies and V. Ogryzko, M. Lipinski, and P. Adams for the kind gift of anti-HIRA antibodies.

This work was supported by grants 4470 (C.M.) and 3828 (F.O.) from the Association de Recherche contre le Cancer and by the CEA/Institut Curie Programme Incitatif et Coopératif on Epigenetic Parameters in DNA Damage Response and the Cell Cycle.

REFERENCES

1. **Adkins, M. W., and J. K. Tyler.** 2004. The histone chaperone Asf1p mediates global chromatin disassembly in vivo. J. Biol. Chem. **279:**52069–52074.
2. **Agez, M., J. Chen, R. Guerois, C. van Heijenoort, J. Y. Thuret, C. Mann, and F. Ochsenbein.** 2007. Structure of the histone chaperone ASF1 bound to the histone H3 C-terminal helix and functional insights. Structure **15:**191–199.
3. **Ahmad, K., and S. Henikoff.** 2002. The histone variant H3.3 marks active chromatin by replication-independent nucleosome assembly. Mol. Cell **9:**1191–1200.
4. **Antczak, A. J., T. Tsubota, P. D. Kaufman, and J. M. Berger.** 2006. Structure of the yeast histone H3-ASF1 interaction: implications for chaperone mechanism, species-specific interactions, and epigenetics. BMC Struct. Biol. **6:**26.
5. **Bravo, R., and H. Macdonald-Bravo.** 1987. Existence of two populations of cyclin/proliferating cell nuclear antigen during the cell cycle: association with DNA replication sites. J. Cell Biol. **105:**1549–1554.
6. **Chow, C. M., A. Georgiou, H. Szutorisz, A. Maia e Silva, A. Pombo, I. Barahona, E. Dargelos, C. Canzonetta, and N. Dillon.** 2005. Variant histone H3.3 marks promoters of transcriptionally active genes during mammalian cell division. EMBO Rep. **6:**354–360.
7. **Cremisi, C., and M. Yaniv.** 1980. Sequential assembly of newly synthesized histones on replicating SV40 DNA. Biochem. Biophys. Res. Commun. **92:**1117–1123.
8. **Daganzo, S. M., J. P. Erzberger, W. M. Lam, E. Skordalakes, R. Zhang, A. A. Franco, S. J. Brill, P. D. Adams, J. M. Berger, and P. D. Kaufman.** 2003. Structure and function of the conserved core of histone deposition protein Asf1. Curr. Biol. **13:**2148–2158.
9. **Earnshaw, W. C., B. M. Honda, R. A. Laskey, and J. O. Thomas.** 1980. Assembly of nucleosomes: the reaction involving *X. laevis* nucleoplasmin. Cell **21:**373–383.
10. **English, C. M., M. W. Adkins, J. J. Carson, M. E. Churchill, and J. K. Tyler.** 2006. Structural basis for the histone chaperone activity of Asf1. Cell **127:**495–508.
11. **Gaillard, P. H., E. M. Martini, P. D. Kaufman, B. Stillman, E. Moustacchi, and G. Almouzni.** 1996. Chromatin assembly coupled to DNA repair: a new role for chromatin assembly factor I. Cell **86:**887–896.
12. **Green, C. M., and G. Almouzni.** 2003. Local action of the chromatin assembly factor CAF-1 at sites of nucleotide excision repair in vivo. EMBO J. **22:**5163–5174.
13. **Green, E. M., A. J. Antczak, A. O. Bailey, A. A. Franco, K. J. Wu, J. R. Yates III, and P. D. Kaufman.** 2005. Replication-independent histone deposition by the HIR complex and Asf1. Curr. Biol. **15:**2044–2049.
14. **Groth, A., A. Corpet, A. J. Cook, D. Roche, J. Bartek, J. Lukas, and G. Almouzni.** 2007. Regulation of replication fork progression through histone supply and demand. Science **318:**1928–1931.
15. **Groth, A., D. Ray-Gallet, J. P. Quivy, J. Lukas, J. Bartek, and G. Almouzni.** 2005. Human Asf1 regulates the flow of S phase histones during replicational stress. Mol. Cell **17:**301–311.
16. **Hake, S. B., B. A. Garcia, E. M. Duncan, M. Kauer, G. Dellaire, J. Shabanowitz, D. P. Bazett-Jones, C. D. Allis, and D. F. Hunt.** 2006. Expression patterns and post-translational modifications associated with mammalian histone H3 variants. J. Biol. Chem. **281:**559–568.
17. **Hoek, M., and B. Stillman.** 2003. Chromatin assembly factor 1 is essential and couples chromatin assembly to DNA replication in vivo. Proc. Natl. Acad. Sci. USA **100:**12183–12188.
18. **Houlard, M., S. Berlivet, A. V. Probst, J. P. Quivy, P. Hery, G. Almouzni, and M. Gerard.** 2006. CAF-1 is essential for heterochromatin organization in pluripotent embryonic cells. PLoS Genet. **2:**e181.
19. **Hu, C. D., and T. K. Kerppola.** 2003. Simultaneous visualization of multiple protein interactions in living cells using multicolor fluorescence complementation analysis. Nat. Biotechnol. **21:**539–545.
20. **Ishimi, Y., J. Hirosumi, W. Sato, K. Sugasawa, S. Yokota, F. Hanaoka, and M. Yamada.** 1984. Purification and initial characterization of a protein which facilitates assembly of nucleosome-like structure from mammalian cells. Eur. J. Biochem. **142:**431–439.
21. **Kaufman, P. D., R. Kobayashi, N. Kessler, and B. Stillman.** 1995. The p150 and p60 subunits of chromatin assembly factor I: a molecular link between newly synthesized histones and DNA replication. Cell **81:**1105–1114.
22. **Kimura, H., and P. R. Cook.** 2001. Kinetics of core histones in living human cells: little exchange of H3 and H4 and some rapid exchange of H2B. J. Cell Biol. **153:**1341–1353.
23. **Krude, T.** 1995. Chromatin assembly factor 1 (CAF-1) colocalizes with replication foci in HeLa cell nuclei. Exp. Cell Res. **220:**304–311.
24. **Laskey, R. A., and W. C. Earnshaw.** 1980. Nucleosome assembly. Nature **286:**763–767.
25. **Le, S., C. Davis, J. B. Konopka, and R. Sternglanz.** 1997. Two new S-phase-specific genes from *Saccharomyces cerevisiae*. Yeast **13:**1029–1042.
26. **Loppin, B., E. Bonnefoy, C. Anselme, A. Laurencon, T. L. Karr, and P. Couble.** 2005. The histone H3.3 chaperone HIRA is essential for chromatin assembly in the male pronucleus. Nature **437:**1386–1390.
27. **Loyola, A., and G. Almouzni.** 2004. Histone chaperones, a supporting role in the limelight. Biochim. Biophys. Acta **1677:**3–11.
28. **Luger, K., A. W. Mader, R. K. Richmond, D. F. Sargent, and T. J. Richmond.** 1997. Crystal structure of the nucleosome core particle at 2.8 A resolution. Nature **389:**251–260.
29. **McKittrick, E., P. R. Gafken, K. Ahmad, and S. Henikoff.** 2004. Histone H3.3 is enriched in covalent modifications associated with active chromatin. Proc. Natl. Acad. Sci. USA **101:**1525–1530.
30. **Meshorer, E., D. Yellajoshula, E. George, P. J. Scambler, D. T. Brown, and T. Misteli.** 2006. Hyperdynamic plasticity of chromatin proteins in pluripotent embryonic stem cells. Dev. Cell **10:**105–116.
31. **Mills, A. D., J. J. Blow, J. G. White, W. B. Amos, D. Wilcock, and R. A. Laskey.** 1989. Replication occurs at discrete foci spaced throughout nuclei replicating in vitro. J. Cell Sci. **94:**471–477.
32. **Mousson, F., A. Lautrette, J. Y. Thuret, M. Agez, R. Courbeyrette, B. Amigues, E. Becker, J. M. Neumann, R. Guerois, C. Mann, and F. Ochsenbein.** 2005. Structural basis for the interaction of Asf1 with histone H3 and its functional implications. Proc. Natl. Acad. Sci. USA **102:**5975–5980.
33. **Mousson, F., F. Ochsenbein, and C. Mann.** 2007. The histone chaperone Asf1 at the crossroads of chromatin and DNA checkpoint pathways. Chromosoma **116:**79–93.
34. **Munakata, T., N. Adachi, N. Yokoyama, T. Kuzuhara, and M. Horikoshi.** 2000. A human homologue of yeast anti-silencing factor has histone chaperone activity. Genes Cells **5:**221–233.
35. **Nabatiyan, A., and T. Krude.** 2004. Silencing of chromatin assembly factor 1 in human cells leads to cell death and loss of chromatin assembly during DNA synthesis. Mol. Cell. Biol. **24:**2853–2862.
36. **Nagai, T., K. Ibata, E. S. Park, M. Kubota, K. Mikoshiba, and A. Miyawaki.**

2002. A variant of yellow fluorescent protein with fast and efficient maturation for cell-biological applications. Nat. Biotechnol. **20:**87–90.

37. **Nakamura, H., T. Morita, and C. Sato.** 1986. Structural organizations of replicon domains during DNA synthetic phase in the mammalian nucleus. Exp. Cell Res. **165:**291–297.
38. **Natsume, R., M. Eitoku, Y. Akai, N. Sano, M. Horikoshi, and T. Senda.** 2007. Structure and function of the histone chaperone CIA/ASF1 complexed with histones H3 and H4. Nature **446:**338–341.
39. **Nelson, D. M., X. Ye, C. Hall, H. Santos, T. Ma, G. D. Kao, T. J. Yen, J. W. Harper, and P. D. Adams.** 2002. Coupling of DNA synthesis and histone synthesis in S phase independent of cyclin/cdk2 activity. Mol. Cell. Biol. **22:**7459–7472.
40. **Nollen, E. A., F. A. Salomons, J. F. Brunsting, J. J. Want, O. C. Sibon, and H. H. Kampinga.** 2001. Dynamic changes in the localization of thermally unfolded nuclear proteins associated with chaperone-dependent protection. Proc. Natl. Acad. Sci. USA **98:**12038–12043.
41. **Phair, R. D., S. A. Gorski, and T. Misteli.** 2004. Measurement of dynamic protein binding to chromatin in vivo, using photobleaching microscopy. Methods Enzymol. **375:**393–414.
42. **Polo, S. E., D. Roche, and G. Almouzni.** 2006. New histone incorporation marks sites of UV repair in human cells. Cell **127:**481–493.
43. **Polo, S. E., S. E. Theocharis, J. Klijanienko, A. Savignoni, B. Asselain, P. Vielh, and G. Almouzni.** 2004. Chromatin assembly factor-1, a marker of clinical value to distinguish quiescent from proliferating cells. Cancer Res. **64:**2371–2381.
44. **Prado, F., F. Cortes-Ledesma, and A. Aguilera.** 2004. The absence of the yeast chromatin assembly factor Asf1 increases genomic instability and sister chromatid exchange. EMBO Rep. **5:**497–502.
45. **Ray-Gallet, D., J. P. Quivy, H. W. Sillje, E. A. Nigg, and G. Almouzni.** 2007. The histone chaperone Asf1 is dispensable for direct de novo histone deposition in *Xenopus* egg extracts. Chromosoma **116:**487–496.
46. **Roberts, C., H. F. Sutherland, H. Farmer, W. Kimber, S. Halford, A. Carey, J. M. Brickman, A. Wynshaw-Boris, and P. J. Scambler.** 2002. Targeted mutagenesis of the Hira gene results in gastrulation defects and patterning abnormalities of mesoendodermal derivatives prior to early embryonic lethality. Mol. Cell. Biol. **22:**2318–2328.
47. **Sanematsu, F., Y. Takami, H. K. Barman, T. Fukagawa, T. Ono, K. Shibahara, and T. Nakayama.** 2006. Asf1 is required for viability and chromatin assembly during DNA replication in vertebrate cells. J. Biol. Chem. **281:** 13817–13827.
48. **Schulz, L. L., and J. K. Tyler.** 2006. The histone chaperone ASF1 localizes to active DNA replication forks to mediate efficient DNA replication. FASEB J. **20:**488–490.
49. **Shibahara, K., and B. Stillman.** 1999. Replication-dependent marking of DNA by PCNA facilitates CAF-1-coupled inheritance of chromatin. Cell **96:**575–585.
50. **Sillje, H. H., and E. A. Nigg.** 2001. Identification of human Asf1 chromatin assembly factors as substrates of Tousled-like kinases. Curr. Biol. **11:**1068–1073.
51. **Singer, M. S., A. Kahana, A. J. Wolf, L. L. Meisinger, S. E. Peterson, C. Goggin, M. Mahowald, and D. E. Gottschling.** 1998. Identification of high-copy disruptors of telomeric silencing in *Saccharomyces cerevisiae*. Genetics **150:**613–632.
52. **Smith, S., and B. Stillman.** 1989. Purification and characterization of CAF-I, a human cell factor required for chromatin assembly during DNA replication in vitro. Cell **58:**15–25.
53. **Stokes, D. G., and R. P. Perry.** 1995. DNA-binding and chromatin localization properties of CHD1. Mol. Cell. Biol. **15:**2745–2753.
54. **Tagami, H., D. Ray-Gallet, G. Almouzni, and Y. Nakatani.** 2004. Histone H3.1 and H3.3 complexes mediate nucleosome assembly pathways dependent or independent of DNA synthesis. Cell **116:**51–61.
55. **Tang, Y., M. V. Poustovoitov, K. Zhao, M. Garfinkel, A. Canutescu, R. Dunbrack, P. D. Adams, and R. Marmorstein.** 2006. Structure of a human ASF1a-HIRA complex and insights into specificity of histone chaperone complex assembly. Nat. Struct. Mol. Biol. **13:**921–929.
56. **Tyler, J. K., C. R. Adams, S. R. Chen, R. Kobayashi, R. T. Kamakaka, and J. T. Kadonaga.** 1999. The RCAF complex mediates chromatin assembly during DNA replication and repair. Nature **402:**555–560.
57. **Verreault, A., P. D. Kaufman, R. Kobayashi, and B. Stillman.** 1996. Nucleosome assembly by a complex of CAF-1 and acetylated histones H3/H4. Cell **87:**95–104.
58. **Worcel, A., S. Han, and M. L. Wong.** 1978. Assembly of newly replicated chromatin. Cell **15:**969–977.
59. **Wu, R. S., S. Tsai, and W. M. Bonner.** 1983. Changes in histone H3 composition and synthesis pattern during lymphocyte activation. Biochemistry **22:**3868–3873.
60. **Wu, R. S., S. Tsai, and W. M. Bonner.** 1982. Patterns of histone variant synthesis can distinguish G0 from G1 cells. Cell **31:**367–374.
61. **Zhang, R., M. V. Poustovoitov, X. Ye, H. A. Santos, W. Chen, S. M. Daganzo, J. P. Erzberger, I. G. Serebriiskii, A. A. Canutescu, R. L. Dunbrack, J. R. Pehrson, J. M. Berger, P. D. Kaufman, and P. D. Adams.** 2005. Formation of MacroH2A-containing senescence-associated heterochromatin foci and senescence driven by ASF1a and HIRA. Dev. Cell **8:**19–30.